Magnetic Resonance in Medicine 43:393–402 (2000)

In Vivo MR Measurements of Regional Arterial and Venous Blood Volume Fractions in Intact Rat Brain

Timothy Q. Duong and Seong-Gi Kim*

In vivo measurement of cerebral arterial and venous volume fractions is important to the understanding of brain physiology and function. By using an intravascular perfluorocarbon and ^{19}F NMR at 4.7 T, regional arterial and venous volume fractions from an intact rat brain were resolved based on the pseudodiffusion coefficients, which were $(33 \pm 7) \times 10^{-3}$ and $(0.45 \pm 0.13) \times 10^{-3}$ mm^2/sec (mean ± SD, n = 7) for the fast- and slow-moving component, respectively. By exploiting the linear dependence of the perfluorocarbon ^{19}F $1/T_1$ on the dissolved paramagnetic oxygen concentration, combined inversion-recovery and diffusion measurements were made to correlate the short T_1 (high-oxygenation) component with the fast-moving component and the long T_1 (low-oxygenation) component with the slow-moving component. The arterial blood volume fraction was 29 ± 7% of the total cerebral blood volume. Finally, experiments were performed in which different oxygen concentrations were inhaled to validate this technique. Magn Reson Med 43:393–402, 2000. © 2000 Wiley-Liss, Inc.

Key words: perfluorocarbon; oxygen tension; ^{19}F NMR; pseudodiffusion; CBV; BOLD; IVIM

The ability to measure regional arterial and venous blood volume in an intact brain noninvasively has many potential biomedical applications. Arterial and venous blood volumes are important indicators of brain tissue physiology, viability and function. These physiological parameters are carefully regulated under normal conditions. They may change in response to increased neuronal activity and can be drastically perturbed in diseased states such as cerebral ischemia, tumor or edema. Measurement of the cerebral arterial/venous blood volume fractions in a serial and relatively noninvasive manner may prove useful for evaluating cerebral function and pathology in which these physiological parameters are functionally or pathologically altered.

In a technique generally referred to as intravoxel incoherent motion (IVIM) (1,2), an ensemble of spins moving in a random network of small blood vessels will give rise to a diffusion-weighted signal attenuation (1,2). Such a process is referred to as pseudodiffusion to distinguish it from pure diffusion. By using an intravascular perfluorocarbon, Neil and Ackerman (3) demonstrated that the diffusion-weighted ^{19}F intravascular signal in brain was biexponential. They reported the pseudodiffusion coefficient (PDC) of the fast-moving components to be ~80 times that of the slow-moving component. However, according to the authors, "it was not clear what the two components represented" (3). It has been proposed that this biexponential characteristic was the result of the continuous distribution of blood velocities and vessel sizes (4). Henkelman et al. (4) employed a model of hierarchical, self-similar network of blood vessels to model the ^{19}F perfluorocarbon diffusion-weighted data (3). However, the estimated perfusion in the rat brain was an order of magnitude lower than that reported in the literature.

We were intrigued by the marked and distinct difference in magnitude between the two PDCs. We hypothesized that the larger PDC is predominantly associated with the fast-flowing arterial blood, whereas the smaller PDC is predominantly associated with the slow-flowing venous blood. To test this hypothesis, the oxygen-sensitive property of perfluorocarbon was used to determine whether the larger PDC predominantly originates from the more oxygenated arterial compartment and the smaller PDC from the less oxygenated venous compartment.

Perfluorocarbon emulsions are known to be excellent blood substitutes and MR detectable (5,6). They do not cross the blood brain barrier (BBB) and thus serve as intravascular tracers in brain. The spin-lattice relaxation rate constant ($R_1 \equiv 1/T_1$) of the ^{19}F nuclei of a perfluorocarbon is linearly dependent on the dissolved oxygen concentration (5,6). The paramagnetic molecular oxygen is the predominant source of T_1 relaxation in vivo. Thus, these unique PFC properties offer a potentially valuable tool for identifying and measuring relative arterial and venous blood volume in the in vivo brain based on oxygenation differences.

Combined ^{19}F inversion-recovery and pseudodiffusion measurements were made in intact rat brain following the intravenous infusion of a perfluorocarbon to test the above hypothesis. Further, experiments were also performed in which the oxygen concentration of the inhaled gas was modulated to validate this technique. To the best of our knowledge, this study presents the first in vivo MR measurement of regional arterial/venous blood volume fractions and their relative oxygen tension changes in the intact rat brain. This technique can provide a means by which to evaluate these physiological parameters serially and in a relatively noninvasive manner in situ and in vivo. Further, the results of this study also have important implications on the blood oxygenation level dependent (BOLD) functional MRI measurements.

THEORY

Oxygen-sensitive perfluorocarbon emulsion in general does not cross the blood brain barrier to exchange with the extravascular pool when administered intravenously (3).

Center for Magnetic Resonance Research, Department of Radiology, University of Minnesota School of Medicine, Minneapolis, Minnesota.

Grant sponsor: National Institutes of Health; Grant numbers: RR08079; NS38295; NS10930; Grant sponsor: the Whitaker Foundation.

*Correspondence to: Seong-Gi Kim, Ph.D., Center for Magnetic Resonance Research, University of Minnesota School of Medicine, Radiology, 2021 Sixth Street SE, Minneapolis, MN 55455. E-mail: kim@cmrr.umn.edu

Received 7 July 1999; revised 8 November 1999; accepted 11 November 1999.

Relevant to the study herein, we model the cerebral vasculature as a nonexchanging, two-compartment model; namely, the arterial and venous pools. The arterial and venous compartments, which constitute primarily of small arterioles and venules, are defined as the compartments that do not undergo oxygen exchange with the brain tissue. The capillary volume, which undergoes oxygen exchange with tissue, is small (7) and/or is assumed to correspondingly factor into its arterial and venous constituents.

According to the IVIM model (1,2), the two nonexchanging arterial and venous pools of randomly oriented vessels can be characterized by two PDCs (D*). The diffusion-weighted signal attenuation can be written as

$$S_i/S_0 = f_a \exp(-b_i \cdot D^*_a) + (1-f_a)\exp(-b_i \cdot D^*_b), \quad [1]$$

where S_i is the signal amplitude at b_i and S_o is the signal amplitude at $b = 0$. f_a is the fraction (or percent if multiplied by 100) of spins with the larger pseudodiffusion coefficient, D^*_a (the fast-moving component). The remainder of the spins have a smaller pseudodiffusion coefficient, D^*_b (the slow-moving component). The parameter b_i is given by

$$b_i = \gamma^2 G_i^2 \delta^2 (\Delta - \delta/3) \quad [2]$$

where γ is the magnetogyric ratio, G_i is the gradient strength, δ is the duration of each gradient pulse, and Δ is the time between the application of the two gradient pulses. $(\Delta - \delta/3)$ is also known as the diffusion time (t_{diff}) during which the diffusion measurement is sensitive to motion.

Similarly, in principle, the difference in oxygenation between the two nonexchanging vascular pools can give rise to two relaxation time constants (T_1). The inversion recovery (IR) signal behavior can be written as

$$S(TI) = \alpha \exp(-TI/T_{1\alpha}) + (1-\alpha)\exp(-TI/T_{1\beta}) + \Omega \quad [3]$$

where S(TI) is the signal amplitude at an inversion time TI and Ω is a constant; α is the fraction (or percentage) of spins with a shorter T_1 ($T_{1\alpha}$). The remainder of the spins have a longer T_1 ($T_{1\beta}$). Note that the volume fraction α in Eq. [3] and f_a in Eq. [1] are not necessarily the same a priori.

METHODS

In Vitro Calibration

Perfluoro–15–crown–5–ether (Exfluor Research Corp., Round Rock, TX) is a highly sensitive perfluorocarbon with 20 equivalent ^{19}F nuclides, giving rise to one single resonance. High sensitivity is critical because of the small blood volume in the brain. The perfluorocarbon was emulsified into ~200-nm diameter micelles (40% v/v, Gateway Technology Inc., St. Louis, MO). In vitro calibration relating R_1 to O_2 was made using four different gas conditions (0, 21, 31, and 100% O_2 with balance N_2O) bubbled into a pure perfluorocarbon emulsion sample for 30–60 min to equilibrium at 37°C. Two different samples were prepared for each gas condition and two T_1 measurements were made on each sample. The sample temperature was monitored and maintained at 37.0 ± 0.5°C during the T_1 measurement. ^{19}F IR measurements were made using 20 inversion delays (TI). Conversion of percent oxygen to mmHg assumed that 100% oxygen is equal to 760 mmHg. The free diffusion coefficient (D) in a phantom of pure perfluorocarbon emulsion at 37°C was measured using 10 *b*-values with the largest *b*-value of 40,000 sec/mm^2.

Animal Surgery

Seven male Sprague Dawley rats (200–270 g) were anesthetized with ~1% (v/v) halothane in O_2:N_2O gas mixture during surgery and throughout the experiments. Following oral intubation, a jugular vein, a femoral artery, and a femoral vein were catheterized for physiological monitoring, blood gas sampling, and chemical administration. For a better representation of the cerebral venous blood oxygenation, blood gas was sampled via the jugular vein instead of the femoral vein. Arterial blood gas was sampled frequently to ensure a steady state of arterial pO_2 and pCO_2. A capnometer was also employed to monitor the inspired O_2/N_2O and the expired CO_2 of the animals. Heart rate and blood pressure were measured via the femoral artery by using a pressure transducer and a differential amplifier (Acknowledge, Biopac, Santa Barbara, CA). The animal's rectal temperature was monitored and maintained at 37±1° C. While the animal was in the magnet, the pH-balanced, isotonic perfluorocarbon emulsion was administered intravenously (16 ml/kg), while a roughly equal volume of blood was simultaneously withdrawn from the femoral artery over ~1 min.

In four of the seven rats, oxygen concentration of the inhaled gas was modulated without changing the arterial blood gas pCO_2 during the experiment. Two to six different oxygen concentrations were used. It had been shown that hyperoxia does not significantly alter cerebral blood flow (CBF) and metabolism if a constant arterial pCO_2 is maintained (8).

MR Experiments

All MR experiments were performed on a 4.7-T, 40-cm horizontal MRI scanner (Oxford Magnet, Oxford, UK) equipped with a ^{Unity}INOVA console (Varian, Palo Alto, CA), and a homebuilt gradient set (15-G/cm, 150-μsec risetime for all three axes). The same gradient set was used for imaging/voxel selection and diffusion measurements. The animal was carefully secured in a head-holder with ear and bite bars after surgery. A surface coil (1.2 cm in diameter) was positioned on top of the rat head. An image-guided voxel of ~ 8 × 10 × 8 mm^3 was placed at the center of the brain with minimal or no extracerebral and superficial surface vessel signal contamination. Magnetic field homogeneity was optimized in the voxel by ^1H_2O shimming to yield ~12–18 Hz spectral linewidth. All ^{19}F MR spectra were acquired using the volume-localized, double spin-echo point-resolved spectroscopy (PRESS) sequence. The three radiofrequency pulses in the PRESS sequence were 3-msec sinc pulses. A pair of crusher gradients (10 G/cm for 3 msec) were placed around each of the two 180° refocusing pulses to destroy residual transverse magneti-

zation. The ^{19}F IR curve was sampled using logarithmically spaced TIs with $\sim 5 \cdot T_1$ between inversion pulses (10-msec sinc pulse).

Biexponential T_1 and D Measurements*

^{19}F T_1 measurements on a single voxel were made using 64 logarithmically spaced TIs. Four to eight transients were accumulated for signal averaging, yielding a total temporal resolution of 30–60 min. ^{19}F pseudodiffusion measurements were made using the modified PRESS sequence to include the Stejskal-Tanner diffusion measurement scheme (9). A pair of diffusion gradients were placed around each of the two 180° refocusing pulses and the diffusion gradients were turned on in all three principal axes simultaneously, resulting in a total of 6 pairs of diffusion gradients. The sequence parameters were: TE = 42 msec, Δ = 10.6 msec, δ = 6 msec, t_{diff} = 8.6 msec, b = 1, 14, 25, 46, 78, 162, 522, and 1032 sec/mm^2 (see Eq. [2] for definitions). The b-values also included corrections for diffusion-weighting contributions from crusher gradients, voxel selection gradients and cross-gradient interaction (10) among diffusion, voxel selection, and crusher gradients as described elsewhere (9). Four to eight transients were accumulated for signal averaging, yielding a temporal resolution of 15–30 min.

In Vivo Correlation of T_1 Values and PDCs

Combined IR and diffusion measurements were made to correlate the T_1 components with the PDCs by selective signal nulling. Thirty-two logarithmically spaced TI values, up to $5 \cdot T_1$, were used to search for the signal nulls. Following each of the 32 TIs, diffusion measurements were made with seven b-values (1, 14, 25, 36, 212, 417, and 621 sec/mm^2). The null point of the slow-moving component was chosen as the TI value at which the echo amplitudes of the large b-values (212, 417, and 621 sec/mm^2) were at the noise level. The null point of the fast-moving component was chosen as the TI value at which the echo amplitudes of the small b-values (b = 1, 14, 25, and 36 sec/mm^2) were the same as that of the first large b-value (212 sec/mm^2). Two to four transients were accumulated for signal averaging, yielding a temporal resolution of $\sim$ 20 min. At each inversion delay, the PDCs and f_a values were determined by using Eq. [1].

After determining roughly the two TI values at which the signal nulls occurred using the 32 inversion delays, a further search was made by using more densely sampled points (8–15 TI values) around the roughly determined null points. The series of TI values were typically set in steps of $\sim$0.05 sec. Four to eight transients were accumulated for signal averaging, resulting in a temporal resolution of 10–15 min. Typically, 4–6 selective nulling experiments with the high sampling density were performed on each animal. The PDCs and f_a values were determined and averaged for further analysis.

Data Analysis

Inversion recovery data were fitted using the nonlinear least-square method and/or the Bayesian probability theory method (9,11). The diffusion data were plotted as Stejskal-Tanner semilog plots (Eq. [1]) and fitted using the nonlinear least-squares method (ORIGIN 5.0 from Microcal, Northampton, MA). Statistical analysis employed the Student paired t-test and a p-value of 0.05 was generally taken as the criterion for statistical significance unless otherwise specified. All reported values are in means ± standard deviations.

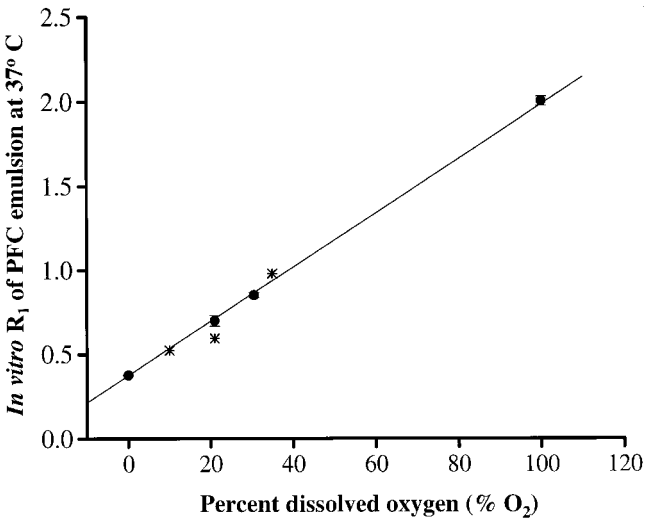

FIG. 1. In vitro standard calibration curve of R_1 at 37°C versus percent dissolved O_2 at four different gas concentrations of 0, 21, 31, and 100% O_2 with balance N_2O. The linear least-squares analysis yielded $R_1 = 0.362 + 0.0163\ O_2$, $R^2 = 0.999$. The error bars indicate the standard deviations (which may be smaller than the data points and thus not visible). The * symbols represent measurements made on the withdrawn arterial blood samples obtained from a rat inhaling three different N_2O:O_2 gas mixture after blood/perfluorocarbon exchange. Only the data points from the pure perfluorocarbon emulsions (not the blood samples) were included in the linear least-squares fit.

RESULTS

In Vitro Measurements

The standard calibration curve for perfluorocarbon ^{19}F R_1 versus percent dissolved oxygen at 37°C is shown in Fig. 1. From linear least-squares analysis

$$R_1 = 0.362 + 0.0163\ O_2,\ R^2 = 0.999 \qquad [4]$$

where O_2 is the percent oxygen bubbled into the solution. In addition, three arterial blood samples were withdrawn from a perfluorocarbon-infused rat after sequentially inhaling three different O_2 concentrations. The perfluorocarbon ^{19}F T_1 of the air-sealed blood samples were measured at 37°C. Blood gas pO_2 was obtained immediately at the end of each T_1 measurement. These results, consistent with the calibration curve using the pure perfluorocarbon emulsion, are plotted as * symbols in Fig. 1.

In vitro diffusion measurements of the perfluorocarbon emulsion in a phantom at 37°C showed only minor signal attenuation with the largest b-value of 40,000 sec/mm^2 (data not shown). The free diffusion coefficient D of the

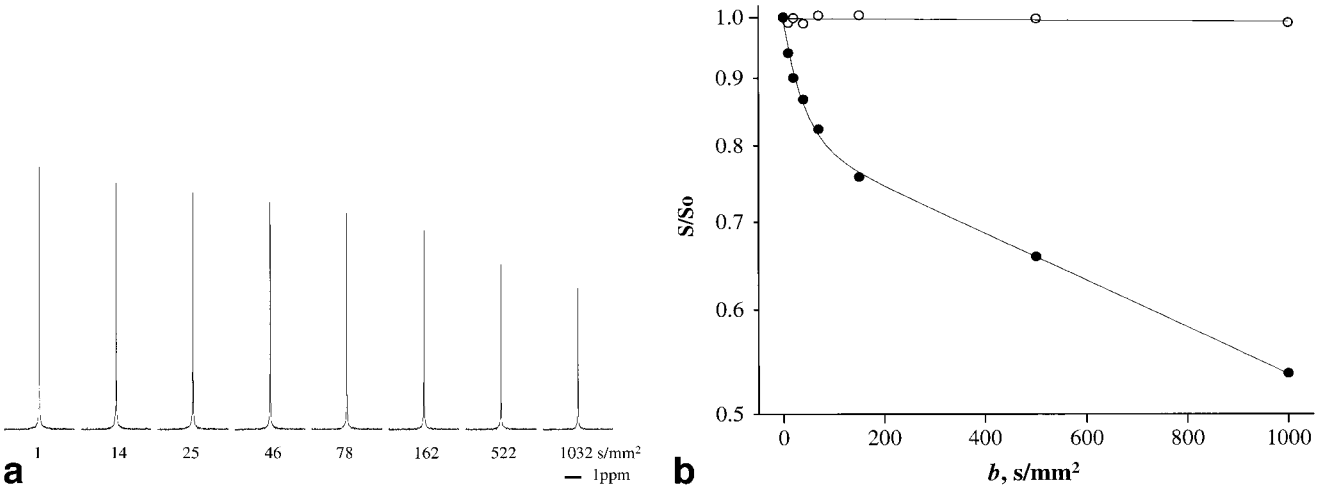

FIG. 2. **a:** Representative series of ^{19}F diffusion-weighted, volume-localized NMR spectra from a live animal. The full-width-at-half-maximum (FWHM) of each spectrum was ~30 Hz. A line broadening of 30 Hz was used. The scale bar indicates the frequency scale of 1 ppm. The number below each spectrum represents the *b*-value (in sec/mm^2) at which the spectrum was obtained. **b:** The semilog Stejskal-Tanner diffusion plot of S/S_o *versus b*-value. Filled circles represent data from a live animal, and open circles represent data from the same animal postmortem. The solid lines are the nonlinear least-squares fits to the data. For the live animal, the biexponential curve fitting gave values of $D^*_a = 20 \times 10^{-3}$ mm^2/sec, $D^*_b = 0.5 \times 10^{-3}$ mm^2/sec, and $f_a = 27\%$. The data points from the dead animal show virtually no signal attenuation at the *b*-values employed. The estimated D* postmortem from the monoexponential fitting is on the order of $\sim 0.001 \times 10^{-3}$ mm^2/sec.

perfluorocarbon emulsion at 37°C was estimated to be ~ 0.001×10^{-3} mm^2/sec.

In Vivo PDC and T_1 Measurements

Following the blood/perfluorocarbon exchange up to ~6 hr, arterial blood gas, mean arterial blood pressure, and heart rate of the animal did not differ significantly from normal values. Following the blood/perfluorocarbon exchange and multiple blood gas sampling, blood hematocrit measurements (from which perfluorocarbon, red blood cells and plasma were clearly distinguishable) showed that the blood hematocrit decreased only slightly from a normal value of ~ 45% to ~ 37% (n = 2) toward the end of the experiments.

Following the blood/perfluorocarbon exchange in the animal, ^{19}F PDCs were measured. Figure 2a shows a representative series of ^{19}F diffusion-weighted, volume-localized spectra from a live animal. The corresponding semilog Stejskal-Tanner diffusion plot of the spectra (• symbol) is shown in Fig. 2b. The diffusion-weighted signal decay was clearly not monoexponential. The data set was best fit by a biexponential function. The PDCs were $D^*_a = 20 \times 10^{-3}$ mm^2/sec and $D^*_b = 0.5 \times 10^{-3}$ mm^2/sec with the volume fraction of component *a*, $f_a = 27\%$. On the other hand, diffusion-weighted signal attenuation from a dead animal was negligible with the given *b*-values (Fig. 2b). The estimated PDC postmortem was on the order of ~ 0.001×10^{-3} mm^2/sec.

In vivo ^{19}F T_1 measurements were made to determine whether the arterial and venous blood can be resolved based on T_1 differences. A representative inversion recovery curve from a live animal is shown in Fig. 3. The data were best fitted by a biexponential model. The estimated parameters were $T_{1\alpha} = 0.16$ sec, $T_{1\beta} = 0.78$ sec, and $\alpha = 13\%$. Based on these in vivo T_1 values, the arterial and venous oxygen tensions estimated via the calibration curve (Eq. [4]) were inconsistent with those obtained via blood gas sampling of 231 and 64 mmHg, respectively. This discrepancy indicated that the in vivo T_1 values were underestimated due to the inflow effect (which effectively

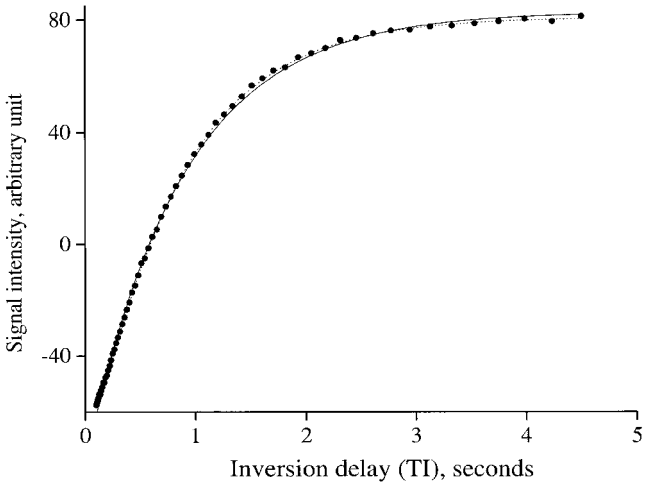

FIG. 3. A representative inversion-recovery curve obtained from a volume-localized voxel. The data are represented in filled circles. The solid line is the fit to a single exponential function. Note the overshoot/undershoot of the fit, which indicates the presence of at least one more exponential component in the data set. The dashed line is the fit to a biexponential function for which excellent correspondence between data and model is observed. Bayesian probability theory estimated the probability for two exponentials in the data set to be 0.999. The estimated parameters were $T_{1\alpha} = 0.16$ s, $T_{1\beta} = 0.78$ s, and $\alpha = 13\%$.

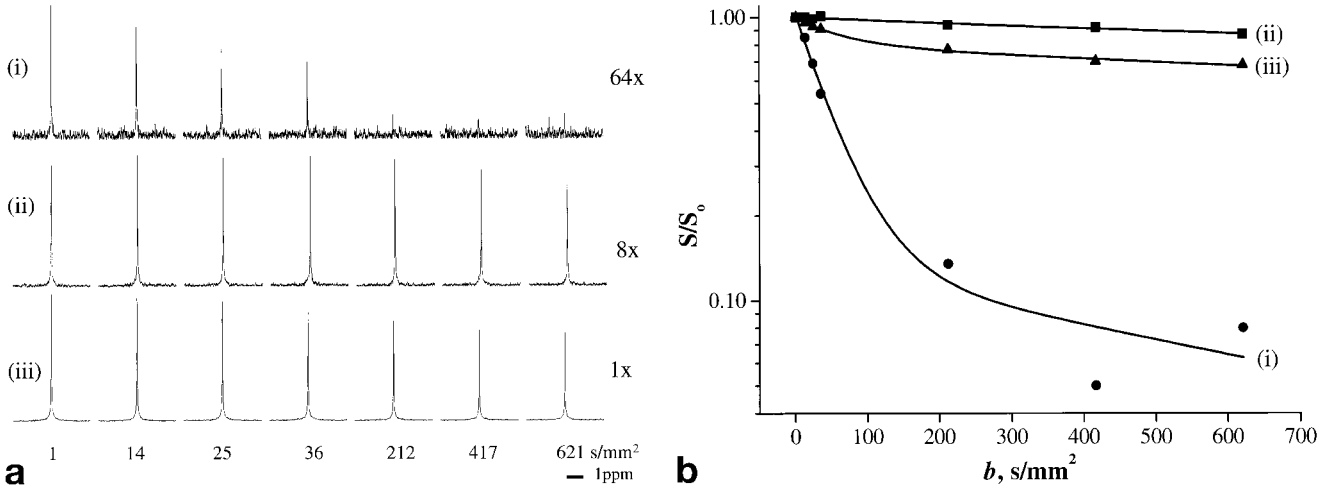

FIG. 4 **a:** Diffusion-weighted spectra obtained with seven *b*-values for three different inversion delays. The scale bar indicates the frequency scale of 1 ppm. The number below each spectrum represents the *b*-value (in sec/mm^2) at which the spectrum was obtained. The notations 1x, 8x and 64x on the right of the spectra indicate the vertical scaling factors. (i) Diffusion-weighted spectra for TI = 0.49 s at which one PDC component was nulled. The signal intensities obtained with the larger *b*-values of 212, 417 and 621 sec/mm^2 are almost at the noise levels. The larger PDC can be determined. (ii) Diffusion-weighted spectra for TI = 0.28 s at which the other PDC component is nulled. The signal intensities obtained with the smaller *b*-values of 1, 14, 25 and 36 sec/mm^2 are roughly equal to that obtained with b = 212 s/mm^2 (the first large *b*-value). The smaller PDC can be determined. (iii) Diffusion-weighted spectra at TI = $5 \cdot T_1$. The signal decay is the weighted average of the "fast" and "slow" pseudodiffusion coefficients. **b:** The corresponding Stejskal-Tanner semilog plots for the spectra shown in Fig. 4a. The first points of all three Stejskal-Tanner plots were normalized to unity for consistency in presentation. The selective nulling of each of the two components was efficient, typically left with ~ 5% residuals.

shortened the measured T_1 values). Following the death of the animal, the inversion recovery data set was best fit by a monoexponential function (data not shown), yielding a postmortem T_1 of 2.80 sec. The averaged ^{19}F T_1 postmortem from all seven animals was 2.85 ± 0.15 sec, consistent with the in vitro T_1 value at 0% oxygen concentration of 2.76 sec.

In Vivo Correlation of T_1 Values and PDCs

Combined IR and diffusion measurements were employed to determine whether the D^*_a and D^*_b were predominantly associated with $T_{1\alpha}$ (more oxygenated arterial component) and $T_{1\beta}$ (less oxygenated venous component), respectively. This was done by selectively nulling the signal contribution from one T_1 component while measuring the PDC of the other component. Figure 4a (i) shows the diffusion-weighted spectra at TI = 0.49 sec at which one PDC component was nulled. The signal intensities at high *b*-values (212, 417, 621 sec/mm^2) were essentially zero (i.e., into the noise level). Consequently, the spins of the slow-moving component did not contribute to the signal intensities at low *b*-values (1, 14, 25, 36 sec/mm^2). The fast-moving PDC, D^*_a, was determined to be 45×10^{-3} mm^2/sec. Similarly, Fig. 4a (ii) shows the diffusion-weighted spectra at TI = 0.28 sec at which the other PDC component was nulled. The signal intensities at low *b*-values (1, 14, 25, 36 sec/mm^2) have similar magnitude as the intensity at b = 212 sec/mm^2 (the first of the high *b*-value). Consequently, the spins of the fast-moving component did not contribute to the signal intensities at high *b*-values (212, 417, 621 sec/mm^2). The slow-moving PDC, D^*_b, was determined to be 0.35×10^{-3} mm^2/sec. Based on the two sets of spectra, the fast-moving D^*_a was identified as having a shorter T_1 ($T_{1\alpha}$ = 0.41) and the slow-moving D^*_b was identified as having a longer T_1 ($T_{1\beta}$ = 0.71).

As a reference, Fig. 4a (iii) shows the diffusion-weighted spectra at TI = $5 \cdot T_1$. The diffusion-weighted signal attenuation is a weighted average of the fast- and slow-moving components. Biexponential fitting of the diffusion data to Eq. [1] yielded $D^*_a = 45 \times 10^{-3}$ mm^2/sec, $D^*_b = 0.5 \times 10^{-3}$ mm^2/sec, and f_a = 25%. These PDCs (obtained via biexponential PDC fitting) were consistent with those obtained via the selective nulling (Fig. 4a, i and ii).

For better visualization, the diffusion-weighted spectra in Fig 4a are plotted as Stejskal-Tanner semilog plots. These are shown in Fig. 4b. The first points of all three Stejskal-Tanner plots were normalized to unity for consistency. The selective nulling of each of the two components was efficient, typically left with ~5% residuals. The small residuals also suggested the absence of additional PDC components.

Table 1 summarizes the average results of the combined IR and diffusion measurements for all animals. The average D^*_a and D^*_b were $(33.3 \pm 7.4) \times 10^{-3}$ mm^2/sec and $(0.45 \pm 0.13) \times 10^{-3}$ mm^2/sec, respectively, as obtained by using the nulling technique. The average D^*_a and D^*_b were $(34.8 \pm 9.3) \times 10^{-3}$ mm^2/sec and $(0.52 \pm 0.13) \times 10^{-3}$ mm^2/sec, respectively, as obtained by using the biexponential fitting of the diffusion data at TI = $5 \cdot T_1$. There were no statistical differences between the PDCs determined via the two methods. The average D^*_a was about 80 times that of D^*_b and they were statistically different from each other ($p < 2 \times 10^{-5}$). The average blood volume fraction of component *a* (f_a) was 29 ± 6% of the total cerebral blood volume.

Table 1
Summary of D_a^*, D_b^* and f_a (Mean ± SD, n = 7)[a]

	D_a^* (10^{-3} mm^2/sec)		D_b^* (10^{-3} mm^2/sec)		f_a (%)[d]
	By nulling[b]	By fitting[c]	By nulling[b]	By fitting[c]	
Rat 1	34.0	30.0	0.47	0.55	36.6
Rat 2	35.0	40.0	0.55	0.65	28.1
Rat 3	39.0	50.0	0.67	0.53	28.6
Rat 4	24.0	27.0	0.29	0.34	17.3
Rat 5	41.0	36.0	0.35	0.52	36.0
Rat 6	38.0	38.5	0.48	0.68	28.5
Rat 7	22.0	22.0	0.34	0.36	31.0
Mean	33.3[e]	34.8[e]	0.45[e]	0.52[e]	29.4
SD	7.4	9.3	0.13	0.13	6.4

[a] The average value of each animal was obtained by first averaging the 4–6 measurements for each arterial pO_2, and then averaging across multiple arterial pO_2 (if applicable). No correlation between the PDC and arterial pO_2 was observed. The average blood gas pCO_2 across different inhaled [O_2] was at 32 ± 5 mmHg.
[b] D_a^* and D_b^* were determined by nulling each of the two components one at a time.
[c] D_a^* and D_b^* were determined by fitting of the diffusion data at $TI = 5 \cdot T_1$.
[d] f_a was determined via biexponential fitting of the diffusion data at $TI = 5 \cdot T_1$.
[e] D_a^* values measured by nulling and by fitting were not statistically different from each other ($p = 0.15$). D_b^* values measured by nulling and by fitting were also not statistically different from each other ($p = 0.50$). D_a^* and D_b^* were statistically different from each other ($p < 2 \times 10^{-5}$). Thus, measurements of PDCs and arterial/venous blood volume fractions can be done by performing diffusion measurements at $TR = 5 \cdot T_1$ followed by biexponential PDC fitting (this is the most time efficient scheme).

Correlation of R_{1a} Versus Arterial pO_2

In order to verify that the short T_1 component is indeed sensitive to changes in arterial oxygen tension, combined IR and diffusion experiments were performed in which the oxygen concentration of the inhaled gas was modulated without changing the arterial blood gas pCO_2. The arterial blood gas pCO_2 was maintained at 32 ± 5 mmHg (ranging from 24 to 38 mmHg for all four animals). Figure 5 shows a representative single-animal plot of R_1 of the fast-moving component (R_{1a}) versus arterial blood gas pO_2. There is clearly a positive linear correlation between R_{1a} and arterial pO_2 ($R_{1a} = 1.7 + 0.015\ O_2$, $R^2 = 0.94$). The slope of 0.015 is consistent with that (0.016) of the calibration curve (Fig. 1). The intercept of this plot, on the other hand, differs from that of the calibration curve, consistent with the notion that the inflow contributed significantly to the measured T_1 value. Table 2 summarizes the slopes and intercepts from the four animals in which the O_2 content of the inhaled gas was modulated. The average slope and intercept were 0.014 ± 0.005 and 2.6 ± 0.7, respectively.

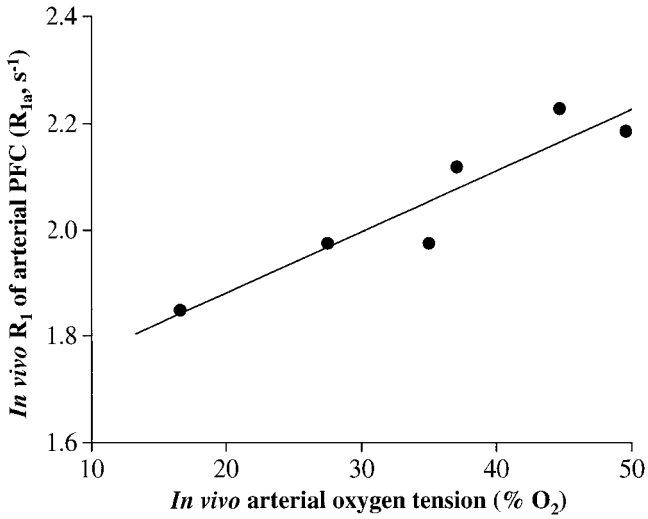

FIG. 5. In vivo perfluorocarbon R_1 of the fast-moving component (R_{1a}) versus arterial oxygen tension. The R_{1a} was determined from the selective nulling MR experiments and the arterial oxygen tension was measured via blood gas sampling. The relationship of the in vivo R_{1a} versus arterial blood gas pO_2 (expressed as % O_2 instead of mmHg) is $R_{1a} = 1.7 + 0.015\ O_2$, $R^2 = 0.94$. The slope is similar to that of the in vitro calibration curve (0.016).

Little or no correlation between the R_1 of the slow-moving component (R_{1b}) and arterial blood gas pO_2 was observed, consistent with the arterial and venous blood gas measurements. This is because the venous blood gas pO_2 changed over a very small range as the arterial blood gas pO_2 was modulated (a direct consequence of the oxygen-binding characteristics of hemoglobin). No correlation between R_{1a} and venous blood gas pO_2 was observed. Similarly, no correlation between R_{1b} and venous blood gas pO_2 was observed.

DISCUSSION

Biocompatibility of Perfluorocarbon

Biocompatibility of perfluorocarbon emulsions as blood substitutes have been extensively reviewed (5,12). Some perfluorocarbons have been approved for human use and still many others are under clinical trials (6). Following substantial (> 50%) blood volume replacement with various perfluorocarbon emulsions, animals are able to survive and develop normally (5). Specifically, perfluoro–15–crown–5–ether emulsion has been previously used to measure pO_2 in mice with tumors and no ill effect was observed (13). Here we found no significant changes in the monitored physiological parameters for up to ~6 hours following the exchange of blood with perfluoro–15–crown–5–ether emulsion in rats. The perfluorocarbon/

Table 2
Slopes and Intercepts of In Vivo R_{1a} Versus Arterial Blood-Gas pO_2 Plot

	Rat 1	Rat 2	Rat 3	Rat 4	Mean ± SD
Slope	0.015	0.007	0.014	0.019	0.014 ± 0.005[a]
Intercept	1.7	2.4	3.2	3.2	2.6 ± 0.7[a]

[a] The average slope of 0.014 is consistent with that obtained from the calibration curve (0.0163). The average intercept of 2.6, on the other hand, differs from that of the calibration curve (0.362). This difference was attributed to the inflow effect (see text).

blood exchange followed by multiple blood samplings decreased hematocrit, resulting in low oxygen delivery efficiency to the tissue. Consequently, the arterial blood gas pO_2 had to be maintained at ~120 mmHg to prevent tissue hypoxia and death. We verified that such a need to maintain arterial $pO_2 \sim 120$ mmHg was largely not due to perfluorocarbon emulsion per se by performing experiments in which roughly equal amounts of blood was replaced by saline followed by multiple blood sampling (n = 3; data not shown). In these experiments, the animals did not survive if the arterial pO_2 was below ~ 120 mmHg. In short, the infusion of 15–crown–5–ether emulsion per se with the dose herein did not significantly perturb normal physiology.

Pseudodiffusion Coefficients in Live Animals Are Dominated by Flow

The free diffusion coefficient D of the pure perfluorocarbon emulsion in a phantom was estimated to be $\sim 0.001 \times 10^{-3}$ mm^2/sec at 37°C, approximately 10^3 times less than that of water ($D_{water} \approx 3 \times 10^{-3}$ mm^2/sec at 37°C). This is consistent with the differences in size and viscosity between the perfluorocarbon emulsion particles and water molecules based on the Stoke-Einstein equation. The D^*_a and D^*_b in the live animal were at least two orders of magnitude larger than the D* in the dead animal, indicating that the PDCs in the live animal were predominantly attributed to flow. In this aspect, perfluorocarbon dynamics is a reasonably good representation of water dynamics in the vasculature of a live animal. Therefore, perfluorocarbon can be used as a marker to mimic intravascular water motion (in the absence of vascular tissue water exchange).

Biexponential Diffusion-Weighted Signal Attenuation

A clear biexponential diffusion-weighted signal decay was observed. The T_1 values obtained via the selective nulling method were clearly correlated with the T_1 values obtained via the biexponential T_1 fitting. Further, the PDCs obtained via the selective nulling method were essentially identical to those obtained via the biexponential fitting of the diffusion data at $TI = 5 \cdot T_1$. These results strongly indicated that the larger PDC is predominantly associated with the more oxygenated arterial pool while the smaller PDC with the less oxygenated venous pool. D^*_a was approximately 80 times that of D^*_b, corresponding to an average "pseudo" root–mean–squared (rms) displacement of a factor of ~ 9. This does not appear to be unreasonable since arterial blood on average is known to be faster-flowing, pulsatile, and more turbulent (larger velocity-to-diameter ratio) relative to venous blood and, thus, arterial blood signals, arising from the random vascular network, are significantly more attenuated by diffusion gradients (14,15). Indeed, biexponential behavior of the diffusion-weighted signal had also been previously observed using a different perfluorocarbon (3). In a study using surface-coil localization on a rat brain and motion-sensitive gradient along the z–axis, Neil and Ackerman reported D^*_a and D^*_b to be 82.4 ± 13 mm^2/sec and 1.02 ± 0.08 mm^2/sec, respectively (3). The D^*_a was also ~ 80 times that of D^*_b in their study even though both D^*_a and D^*_b of Neil and Ackerman were slightly larger than those reported here. Cross-laboratory consistency exists despite the PDCs were measured with motion-sensitive gradients along two different directions; namely, along an oblique axis herein and along the z–axis in their study. This comparison indicated that with sufficiently large voxels (i.e., entire rat brain) employed in both studies, the notion that the MR signals arose from a network of randomly oriented vessels is well justified. The measured PDCs were not biased toward any large numbers of vessels orienting in any given direction. Therefore, the estimated arterial and venous blood volume fractions are unlikely to be significantly different from those estimated by measuring the PDCs in an orientationally averaged fashion.

Henkelman et al. (4) postulated that the biexponential behavior of the PDCs is the result of the continuous hierarchical distribution of blood vessels (without arterial and venous discrimination). Our data do not support the model of a hierarchical network of blood vessels as an explanation for the observed biexponential behavior of the vascular PFC in the brain. Further, the continuous distribution of vessel sizes in the hierarchical network fashion is unlikely to yield two readily resolvable T_1 as well as PDC components. Rather, a continuous distribution of the measured parameters would be expected. Our data suggested that the larger PDC was predominantly arterial in origin, while the smaller PDC was predominantly venous in origin. In all measurements, the fast-moving component correlated with a shorter T_1 (high-oxygenation arterial blood), while the slow-moving component correlated with a longer T_1 (low-oxygenation venous blood). We attributed these marked differences in PDCs to the differences in flow characteristics between the arterial and venous components, which gave rise to a difference in "pseudo" rms displacement of a factor of 9.

Though the use of the simple two-compartment approach to model the cerebral vasculature yields valuable insight into the physiological parameters, it does have drawbacks. For example, this simple model does not account for the gradual transition of flow characteristics and

oxygen tension in the capillaries. This is justified since the capillary volume is known to be small (7). Our data are consistent with this notion. If the capillary contribution were dominant, it is very unlikely that such marked differences in ^{19}F T_1 as well as PDC could be observed. Rather, a continuous distribution of these parameters would be expected. The fact that such marked differences in ^{19}F T_1 and pseudodiffusion coefficients were observed clearly indicated that the capillary signal contribution from the gradual transition of arterial to venous blood was minor. By the same token, these data also indicated that the motion in vessels, larger than capillaries (i.e., arterioles and venules), also exhibited IVIM characteristics. IVIM behavior is expected as long as these relatively larger blood vessels are randomly oriented and numerous such that the spins lose their phase memory in the period during which the measurement is sensitive to motion.

Relative Arterial/Venous Blood Volume and Oxygenation

The relative blood volume of the fast-moving arterial component was 29 ± 6%, consistent with that reported by Neil and Ackerman of 29.4 ± 4.3% (3). The arterial blood volume fraction could be underestimated by the T_2 effect arising from oxygenation and characteristic flow differences between the arterial and venous compartments. The ^{19}F T_2 of the arterial and venous blood were ~ 155 msec (160 mmHg) and ~ 180 msec (60 mmHg), respectively, based on the standard calibration curve of $1/T_2$ versus percent O_2 (data not shown). These T_2 differences are expected to result in <4% error in the estimated arterial blood volume. On the other hand, the T_2 effect arising from the characteristic flow differences on the arterial blood volume estimate is unknown and remains to be investigated.

Despite the importance of arterial and venous blood volume measurements in physiology, BOLD modeling (16), and PET oxygen consumption measurement (17), there are only a few literature reports on the arterial and venous blood volume fractions. This is due to the lack of in vivo techniques to perform these measurements. The in vitro histological methods generally suffer from substantial artifacts and are labor intensive. The arterial blood volume fraction had been reported to be 16% (7), 21% (18) and 15% (19). Our value is likely to be the upper limit because it included part of the capillary volume.

Even though quantitative estimates of the arterial and venous oxygen tension were not obtained by the present MR measurements, changes in arterial pO_2 were correctly tracked by this technique, as indicated by the slope in Fig. 5. The intercept of Fig. 5, on the other hand, differed from that of the calibration curve, indicating that the measured T_1 value was contaminated by flow. Note that the inflow effect on the T_1 values in the IR and the selective nulling measurements could be different because of the differences in inversion delays inherent in the two methods. The inflow effect in the IR measurement would be more pronounced because of the relatively longer inversion delays. This is consistent with the fact that the $R_{1\alpha}$ of Fig. 3 was larger than the intercept $R_{1\alpha}$ of Fig. 5. The use of a "whole-body" rat coil could eliminate or reduce the inflow effect on T_1.

Interestingly, the total blood volume in rat brain can be estimated from the flow-contaminated apparent T_1 ($T_{1\ app}$). The measured $T_{1\ app}$ in vivo is quantitatively related to the volumetric flow and the "true" T_1 ($T_{1\ true}$) by

$$1/T_{1\ app} = 1/T_{1\ true} + F/V, \quad [5a]$$

where F is volumetric flow (ml blood/sec) and V is the blood volume in a voxel from which the ^{19}F signal was obtained. The volumetric blood flow is the CBF (in ml blood/g tissue/sec) multiplied by tissue weight from which CBF is measured. Using a CBF value of ~ 1 ml/g tissue/min (20) and assuming the tissue volume of interest (~ $8 \times 10 \times 8$ mm^3) corresponds to 80% tissue weight (i.e., 0.64 ml × 0.8 g/ml), the volumetric flow F was calculated to be 0.0085 ml/sec. By using the arterial $T_{1\ app}$ (the intercept in Table 2) and the $T_{1\ true}$ (the intercept of Fig. 1), the estimated V is that of arterial blood volume,

$$V_{(\text{arterial})} = \frac{F}{1/T_{1\ \text{app(arterial)}} - 1/T_{1\ \text{true}}} = \frac{0.0085\ \text{ml/s}}{2.6\ \text{s}^{-1} - 0.362\ \text{s}^{-1}} = 0.0038\ \text{ml}, \quad [5b]$$

for the given voxel. This arterial blood volume corresponds to ~ 0.6% [= 0.0038 ml/0.64 ml] of the total brain volume. Since the arterial blood volume was 29.4% (Table 1), the total (arterial and venous) blood volume was thus ~ 2%, consistent with those (2–5%) reported in the literature (21–23).

Little or no correlation between the venous R_{1b} and the arterial blood gas pO_2 was observed. This is consistent with the well-known oxygen-binding properties of hemoglobin. Consider the case in which the animal breathes 21% (normoxia) and 100% (hyperoxia) oxygen, the arterial oxygen tension, respectively, increases from ~ 160 to ~ 300 mmHg while the hemoglobin oxygen saturation increases only from ~98 to 100%. Since oxygen consumption and CBF remains relatively constant under hyperoxia (8), the oxygen delivered to the venous side increases only by ~2% following a large increase in arterial pO_2 from normoxia to hyperoxia. It is therefore not surprising that, with such small change in venous pO_2, little or no correlation was observed between the MR-measured venous pO_2 and the modulated arterial pO_2.

It is important to note that the above reasoning assumed hemoglobin is the dominant oxygen carrier. This is still true following the blood/perfluorocarbon exchange. The oxygen-carrying capacity of the pure perfluoro–15–crown–5–ether emulsion was measured to be 10–20 times less efficient than that of hemoglobin under physiological conditions (unpublished data). Further, with the small blood/perfluorocarbon volume exchange and the resultant small hematocrit decrease, the oxygen-carrying capacity contributed by the perfluorocarbon emulsion is negligible and can thus be ignored.

Implications on BOLD fMRI Measurements

Pseudodiffusion coefficient measurements are also of interest in the context of the BOLD fMRI measurements.

BOLD fMRI (24), in which ^1H_2O MR image intensity is dependent on regional vascular oxygenation, has been widely utilized to map human brain functions (25–27). It is well known that with the typical fMRI acquisition parameters and especially at low magnetic field, the BOLD response is particularly sensitive in and around large vessels (i.e., veins), which can be quite distant from the sites of neuronal activity. For example, it has been demonstrated that the BOLD signal at 1.5 T arises predominantly from large vessels (28,29).

It has been proposed that flow-crushing diffusion gradients [similar or identical to that used in diffusion measurement (30)] can be used to reduce or eliminate the intravenous contribution to the BOLD response (28,29,31–33). To date, the flow-crushing gradients typically employed *b*-values of $\sim$ 100 sec/mm^2 with a maximum of $\sim$ 600 sec/mm^2. Our data showed that the fast-moving arterial component of the perfluorocarbon was attenuated to approximately e–fold (37% of the original signal) with a *b*-value of 30 sec/mm^2. However, the slow-moving venous component of the perfluorocarbon was not significantly attenuated ($<$1.5%) with such a *b*-value. Further, the venous component shows only $\sim$ 25% signal attenuation with a *b*-value as high as 600 sec/mm^2. Since the BOLD response is predominantly of venous (as opposed to arterial) origin, these data strongly indicate that the flow-crushing gradient technique (with *b*-value up to 600 sec/mm^2) would not eliminate the intravenous contribution to the BOLD response (even though flow-crushing gradients do attenuate the signal contributions from large vessels relative to small ones).

CONCLUSIONS

In this study, we demonstrated for the first time that regional arterial and venous blood volume fractions can be noninvasively measured in an intact rat brain in vivo. By using the oxygen-sensitive property of perfluorocarbon, we correlated the fast- and slow-moving components with the more oxygenated arterial and less oxygenated venous components, respectively. This technique can readily be applied to measure changes in cerebral oxygen tension, oxygen consumption, total and relative arterial/venous blood volume in association with functional stimulation. With the existing clinically approved perfluorocarbons, these measurements can potentially be made in humans.

ACKNOWLEDGMENTS

The authors thank Prof. Christopher H. Sotak of the Worcester Polytechnic Institute for valuable suggestions, Dr. G. Larry Bretthorst of the Washington University for providing the Bayesian probability code, and Dr. Hellmut Merkle for maintenance of the spectrometer.

REFERENCES

1. Le Bihan D. Molecular diffusion nuclear magnetic resonance imaging. Magn Reson Q 1991;7:1–30.
2. Le Bihan D, Breton E, Lallemand D, Aubin ML, Vitnaud J, Laval-Jeantet M. Separation of diffusion and perfusion in intravoxel incoherent motion MR imaging. Radiology 1988;168:497–505.
3. Neil JJ, Ackerman JJH. Detection of pseudodiffusion in rat brain following blood substitution with perfluorocarbon. J Magn Reson 1992;97:194–201.
4. Henkelman RM, Neil JJ, Xiang Q-S. A quantitative interpretation of IVIM measurements of vascular perfusion in the rat brain. Magn Reson Med 1994;32:464–469.
5. Riess J, Maurice LB. Perfluoro compounds as blood substitute. Angewandte Chemie 1978;17:621–634.
6. Lowe KC. Perfluorocarbons as oxygen-transport fluids. Comp Biochem Physiol 1987;87:825–838.
7. Rushmer R. Cardiovascular dynamics. Philadelphia: W.B. Saunders Company; 1976. p 8.
8. Kety SS, Schmidt CF. The effects of altered arterial tensions of carbon dioxide and oxygen on cerebral blood flow and cerebral oxygen consumption of normal young men. J Clin Invest 1948;27:484–491.
9. Duong T. Biophysical mechanism(s) of diffusion-weighted magnetic resonance image contrast associated with brain injury in vivo. Ph.D. thesis. St. Louis: Washington University; 1998.
10. Neeman N, Freyer JP, Sillerud LO. Effects of the imaging gradients on the determination of diffusion coefficients. J Magn Reson 1990;90:303–312.
11. Neil JJ, Bretthorst GL. On the use of Bayesian probability theory for analysis of exponential decay. Magn Reson Med 1993;29:642–647.
12. Faithfull NS. Artificial oxygen carrying blood substitutes. Adv Exp Med Biol 1992;317:55–72.
13. Dardzinski BJ, Sotak CH. Rapid tissue oxygen tension mapping using 19F inversion recovery echo planar imaging of perfluoro–15–crown–5–ether. Magn Reson Med 1994;32:88–97.
14. Ahn CB, Lee SY, Nalcioglu O, Cho ZH. The effects of random directional distributed flow in nuclear magnetic resonance imaging. Med Phys 1987;14:43.
15. Grover T, Singer JR. NMR spin-echo flow measurements. J Appl Physiol 1971;42:938.
16. van Zijl PC, Eleff SM, Ulatowski JA, Oja JM, Ulug AM, Traystman RJ, Kauppinen RA. Quantitative assessment of blood flow, blood volume and blood oxygenation effects in functional magnetic resonance imaging. Nat Med 1998;4:159–167.
17. Mintun M, Raichle M, Martin W, Herscovitch P. Brain oxygen utilization measured with O-15 radiotracers and positron emission tomography. J Nucl Med 1984;177–187.
18. Leenders KL, Perani D, Lammertsma AA, Heather JD. Cerebral blood flow, blood volume and oxygen. Brain 1990;113:27–47.
19. Tomita M, Gotoh F, Amano T. Transfer function through regional cerebral cortex evaluated by a photoelectric method. Am J Physiol 1983;245:H385–H398.
20. Tsekos NV, Zhang F, Merkle H, Nagayama M, Iadecola C, Kim S-G. Quantitative measurements of cerebral blood flow in rats using the FAIR technique: Correlation with previous iodoantipyrine autoradiographic studies. Magn Reson Med 1998;39:564–573.
21. Nakagawa H, Lin S-Z, Bereczki D, Gesztelyi G, Otsuka T, Wei L, Hans F-J, Acuff VR, Chen J-L, Pettigrew KD, Patlak CS, Blasberg RG, Fenstermacher JD. Blood volumes, hematocrits, and transit-times in parenchymal microvascular systems of the rat brain. In: Le Bihan D, editor. Diffusion and perfusion magnetic resonance imaging. Application to functional MRI. New York: Raven Press; 1995. p 193-204.
22. Grubb RL, Raichle ME, Eichling JO, Ter-Pogossian MM. The effects of changes in PaCO2 on cerebral blood volume, blood flow, and vascular mean transit time. Stroke 1974;5:630–639.
23. Cremer J, Seville M. Regional brain blood flow, blood volume, and haematocrit values in the adult rat. J Cereb Blood Flow Metab 1983;3:254–256.
24. Ogawa S, Lee T-M, Nayak AS, Glynn P. Oxygenation-sensitive contrast in magnetic resonance image of rodent brain at high magnetic fields. Magn Reson Med 1990;14:68–78.
25. Ogawa S, Tank DW, Menon R, Ellermann JM, Kim S-G, Merkle H, Ugurbil K. Intrinsic signal changes accompanying sensory stimulation: functional brain mapping with magnetic resonance imaging. Proc Natl Acad Sci USA 1992;89:5951–5955.
26. Kwong KK, Belliveau JW, Chesler DA, Goldberg IE, Weisskoff RM, Poncelet BP, Kennedy DN, Hoppel BE, Cohen MS, Turner R, Cheng

H-M, Brady TJ, Rosen BR. Dynamic magnetic resonance imaging of human brain activity during primary sensory stimulation. Proc Natl Acad Sci USA 1992;89:5675–5679.
27. Bandettini PA, Wong EC, Hinks RS, Rikofsky RS, Hyde JS. Time course EPI of human brain function during task activation. Magn Reson Med 1992;25:390–397.
28. Song AW, Wong EC, Tan SG, Hyde JS. Diffusion-weighted fMRI at 1.5T. Magn Reson Med 1996;35:155–158.
29. Boxerman JL, Bandettini PA, Kwong KK, Baker JR, Davis TL, Rosen BR, Weisskoff RM. The intravascular contribution to fMRI signal change: Monte Carlo modeling and diffusion-weighted studies in vivo. Magn Reson Med 1995;34:4–10.
30. Stejskal EO, Tanner JE. Spin diffusion measurements: Spin echoes in the presence of a time-dependent field gradient. J Chem Phys 1965;42: 288–292.
31. Menon RS, Hu X, Adriany G, Andersen P, Ogawa S, Ugurbil K. Comparison of SE-EPI, ASE-EPI and conventional EPI applied to functional neuroimaging: The effect of flow crushing gradients on the BOLD signal. Proc Soc Magn Reson 1994;2:622.
32. Silva AC, Zhang W, Williams DS, Koretsky AP. Estimation of water extraction fractions in rat brain using magnetic resonance measurement of perfusion with arterial spin labeling. Magn Reson Med 1997;37:58–68.
33. Lee S-P, Silva AC, Ugurbil K, Kim S-G. Diffusion-weighted spin-echo fMRI at 9.4 T: microvascular/tissue contribution to BOLD signal change. Magn Reson Med 1999;42:919–928.